

GRAVITATIONAL LENSING

TIME-DELAY COSMOLOGY

R. Benton Metcalf
2022-2023

TIME-DELAYS & THE HUBBLE PARAMETER

time-delay between strongly lensing images

$$\Delta t(\theta) = \frac{D_l D_s}{c D_{ls}} (1 + z_l) \left[\frac{1}{2} |\theta - \beta|^2 - \psi(\theta) \right]$$

$$\Delta t(\theta) \propto \frac{1}{H_o}$$

TIME-DELAYS & THE HUBBLE PARAMETER

measurements of the time-delay

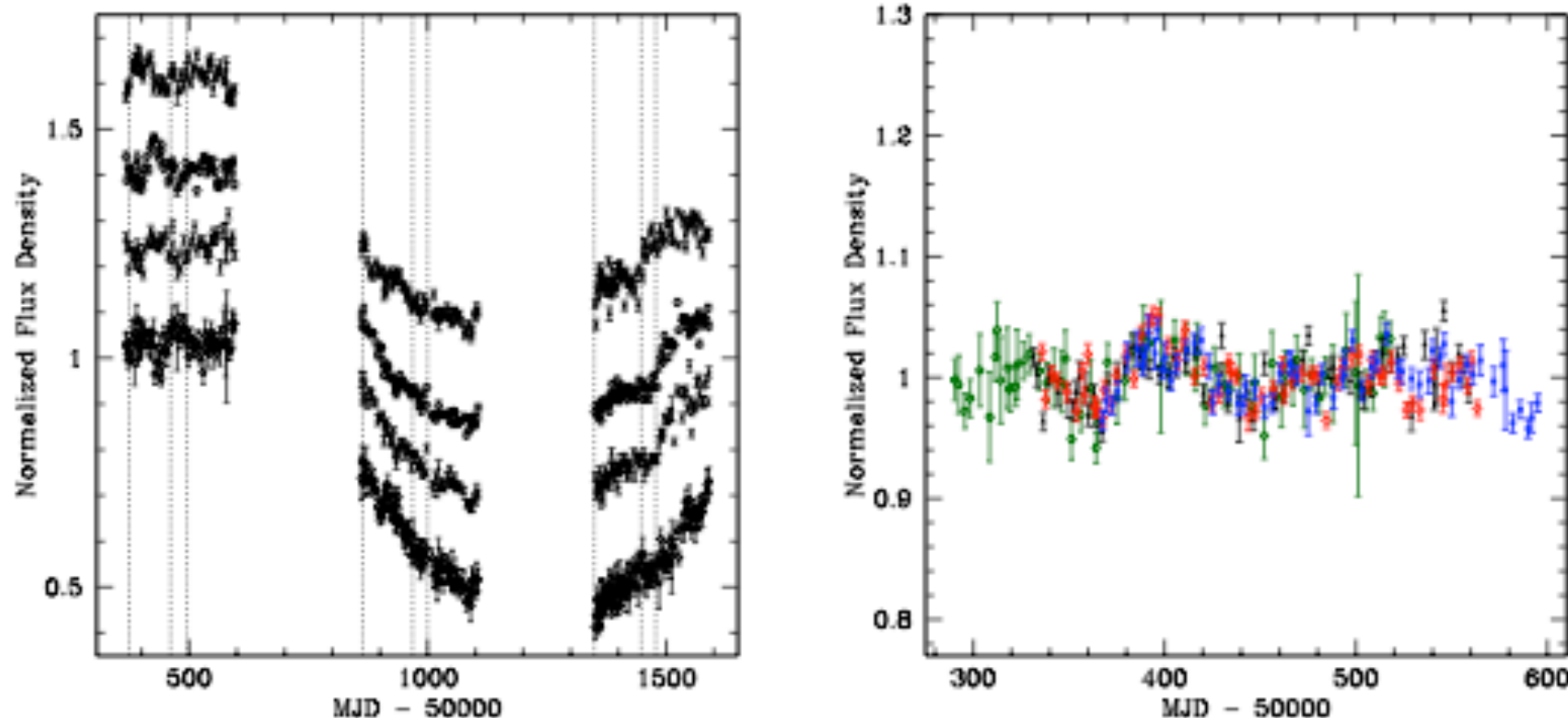


Fig. 1.2. VLA monitoring data for the four-image lens B1608+656. The left panel shows (from top to bottom) the normalized light curves for the B (filled squares), A (open diamonds), C (filled triangles) and D (open circles) images as a function of the mean Julian day. The right panel shows the composite light curve for the first monitoring season after cross correlating the light curves to determine the time delays ($\Delta t_{AB} = 31.5 \pm 1.5$, $\Delta t_{CB} = 36.0 \pm 1.5$ and $\Delta t_{DB} = 77.0 \pm 1.5$ days) and the flux ratios. (From Fassnacht et al. 2002.)

TIME-DELAYS & THE HUBBLE PARAMETER

measurements of the time-delay

C. S. Kochanek and P. L. Schechter

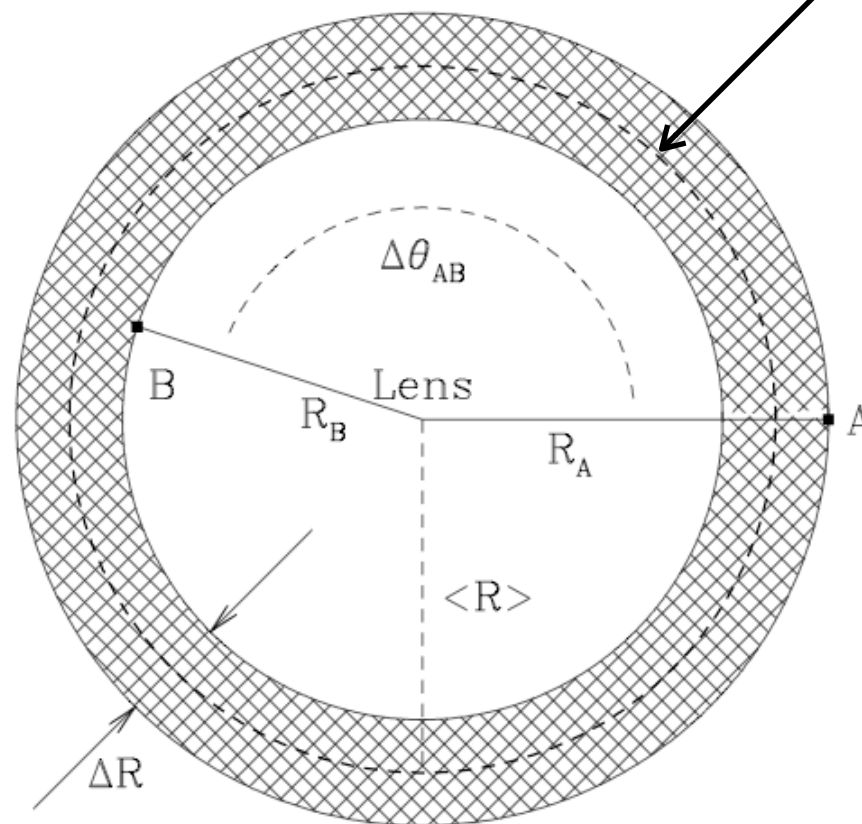
Table 1.1. *Time Delay Measurements*

System	N_{im}	Δt (days)	Astrometry	Model	Ref.
HE1104–1805	2	161 ± 7	+	“simple”	1
PG1115+080	4	25 ± 2	+	“simple”	2
SBS1520+530	2	130 ± 3	+	“simple”	3
B1600+434	2	51 ± 2	+/-	“simple”	4
HE2149–2745	2	103 ± 12	+	“simple”	5
RXJ0911+0551	4	146 ± 4	+	cluster/satellite	6
Q0957+561	2	417 ± 3	+	cluster	7
B1608+656	4	77 ± 2	+/-	satellite	8
B0218+357	2	10.5 ± 0.2	-	“simple”	9
PKS1830–211	2	26 ± 4	-	“simple”	10
B1422+231	4	(8 ± 3)	+	“simple”	11

TIME-DELAYS & THE HUBBLE PARAMETER

Kochanek's formula for time delay between images A and B

$$\Delta t_{AB} = \frac{D_l D_s}{c D_{ls}} (1 + z_l) (|\theta_A|^2 - |\theta_B|^2) \left[1 - \langle \kappa \rangle + \mathcal{O} \left(\frac{|\theta_A| - |\theta_B|}{|\theta_A| + |\theta_B|} \right) \right]$$



*average convergence
in annulus*

TIME-DELAYS & THE HUBBLE PARAMETER

~10 measured time-delays

A number of systematic errors complicate the measurement of the Hubble parameter

Mass-sheet degeneracy

Radial profile degeneracy

Microlensing

Complicated multi-component lenses

Most QSOs are not very variable in the radio where microlensing is small

TIME-DELAYS & THE HUBBLE PARAMETER

COSMOGRAIL - *the Cosmological Monitoring of Gravitational Lenses*

Monitors gravitational lenses in the visible using five telescopes distributed around the world

WFI J2033–4723 - quad lens monitored for three years

for comparison

$$\Delta t_{AB} = 35.5 \pm 1.4 \text{ days}$$

HST Key Project

$$\Delta t_{BC} = 62.6 \pm 4 \text{ days}$$

$$H_o = 73 \pm 8 \text{ km s}^{-1} \text{ Mpc}^{-1}$$

WMAP 5-year +SNe +BAO

$$H_o = 67^{+13}_{-10} \text{ km s}^{-1} \text{ Mpc}^{-1}$$

$$H_o = 70.5 \pm 1.3 \text{ km s}^{-1} \text{ Mpc}^{-1}$$

$$H_o = 63^{+7}_{-3} \text{ km s}^{-1} \text{ Mpc}^{-1} \quad \leftarrow \quad \textit{if isothermal profile is assumed}$$

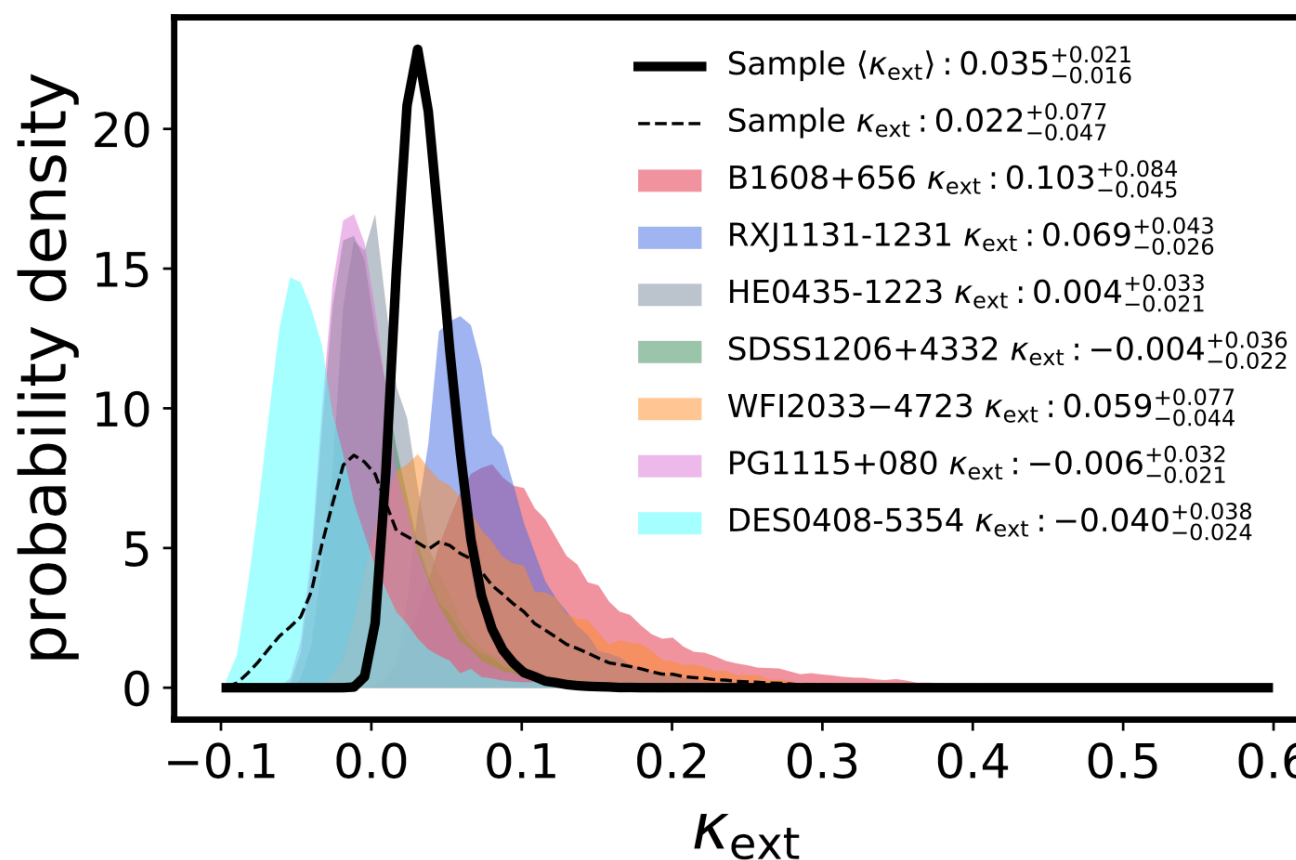
TIME-DELAYS & THE HUBBLE PARAMETER

Birrer et al 2020

name	z_{lens}	z_{source}	r_{eff} [arcsec]	θ_E [arcsec]	γ_{pl}	κ_{ext}	$D_{\Delta t}^{\text{pl}}$ [Mpc]
B1608+656	0.6304	1.394	0.59 ± 0.06	0.81 ± 0.02	2.08 ± 0.03	$+0.103^{+0.084}_{-0.045}$	4775^{+138}_{-130}
RXJ1131-1231	0.295	0.654	1.85 ± 0.05	1.63 ± 0.02	1.95 ± 0.05	$+0.069^{+0.043}_{-0.026}$	1947^{+35}_{-35}
HE0435-1223	0.4546	1.693	1.33 ± 0.05	1.22 ± 0.05	1.93 ± 0.02	$+0.004^{+0.032}_{-0.021}$	2695^{+159}_{-157}
SDSS1206+4332	0.745	1.789	0.34 ± 0.05	1.25 ± 0.01	1.95 ± 0.05	$-0.004^{+0.036}_{-0.021}$	5846^{+628}_{-608}
WFI2033-4723	0.6575	1.662	1.41 ± 0.05	0.94 ± 0.02	1.95 ± 0.02	$+0.059^{+0.078}_{-0.044}$	4541^{+134}_{-152}
PG1115+080	0.311	1.722	0.53 ± 0.05	1.08 ± 0.02	2.17 ± 0.05	$-0.006^{+0.032}_{-0.021}$	1458^{+117}_{-115}
DES0408-5354	0.597	2.375	1.20 ± 0.05	1.92 ± 0.01	1.90 ± 0.03	$-0.040^{+0.037}_{-0.024}$	3491^{+75}_{-74}

external shear

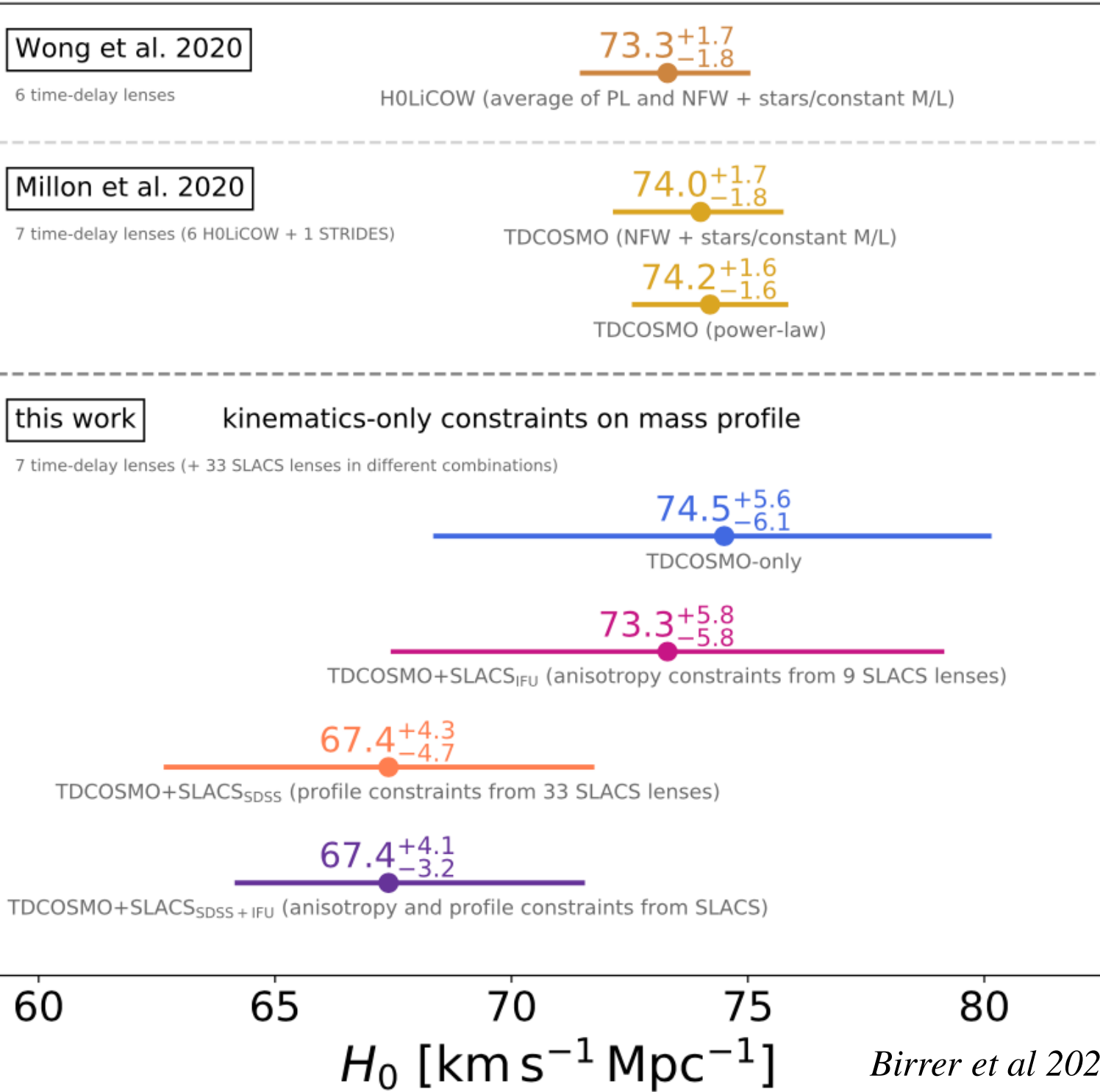
$$D_{\Delta t} = (1 + z + l) \frac{D_l D_s}{D_{ls}}$$



time-delay distance

TIME-DELAYS & THE HUBBLE PARAMETER

H_0 measurements in flat Λ CDM - performed blindly



WMAP 5-year +SNe +BAO

$$H_o = 70.5 \pm 1.3 \text{ km s}^{-1} \text{ Mpc}^{-1}$$

Birrer et al 2020

MASS PROFILE & SHAPE OF GALAXIES

Results from SLACS

Combines internal kinematics with lensing mass for elliptical galaxies.

- *Profile is not consistent with a model where mass follows light*
- *The mass profiles (baryons + dark matter) are consistent with an Isothermal profile*
- *Profiles do not seem to evolve significantly with redshift*
- *There does seem to be small scatter in the slope of the profiles, but it does not seem to be correlated with any property of the visible component of the lens.*
- *The direction of the visible galaxy's ellipticity is aligned with that of the dark matter*
- *The strong and weak lensing data is consistent with the Isothermal profile extending out from a 10s of kpc to a few 100 kpc in these galaxies.*

MASS PROFILE & SHAPE OF GALAXIES

Results from SLACS

$$\rho(r) \propto r^{-\gamma'}$$

The mass profiles (baryons + dark matter) are consistent with an Isothermal profile

Profiles do not seem to evolve significantly with redshift

There does seem to be small scatter in the slope of the profiles, but it does not seem to be correlated with any property of the visible component of the lens.

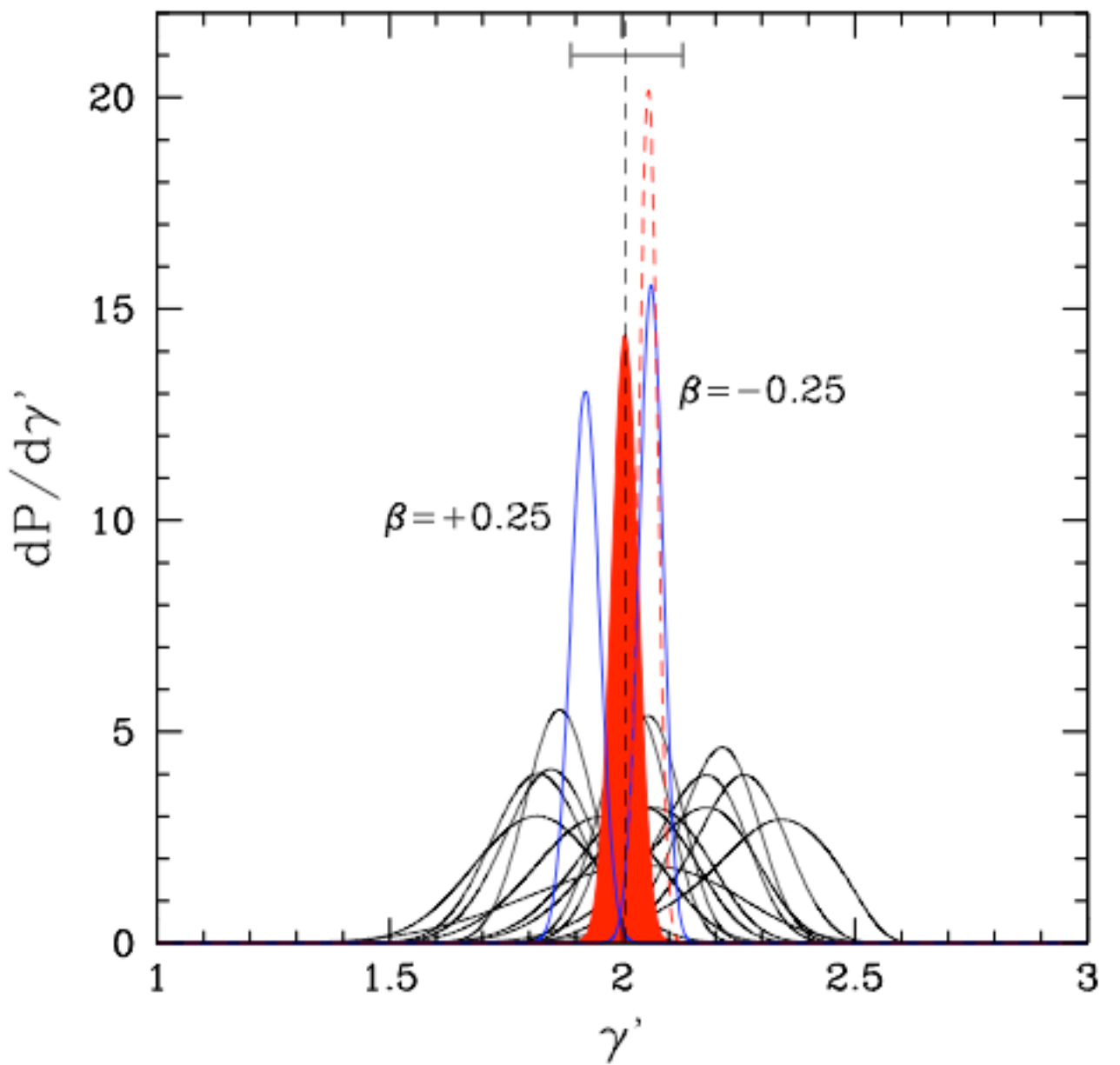
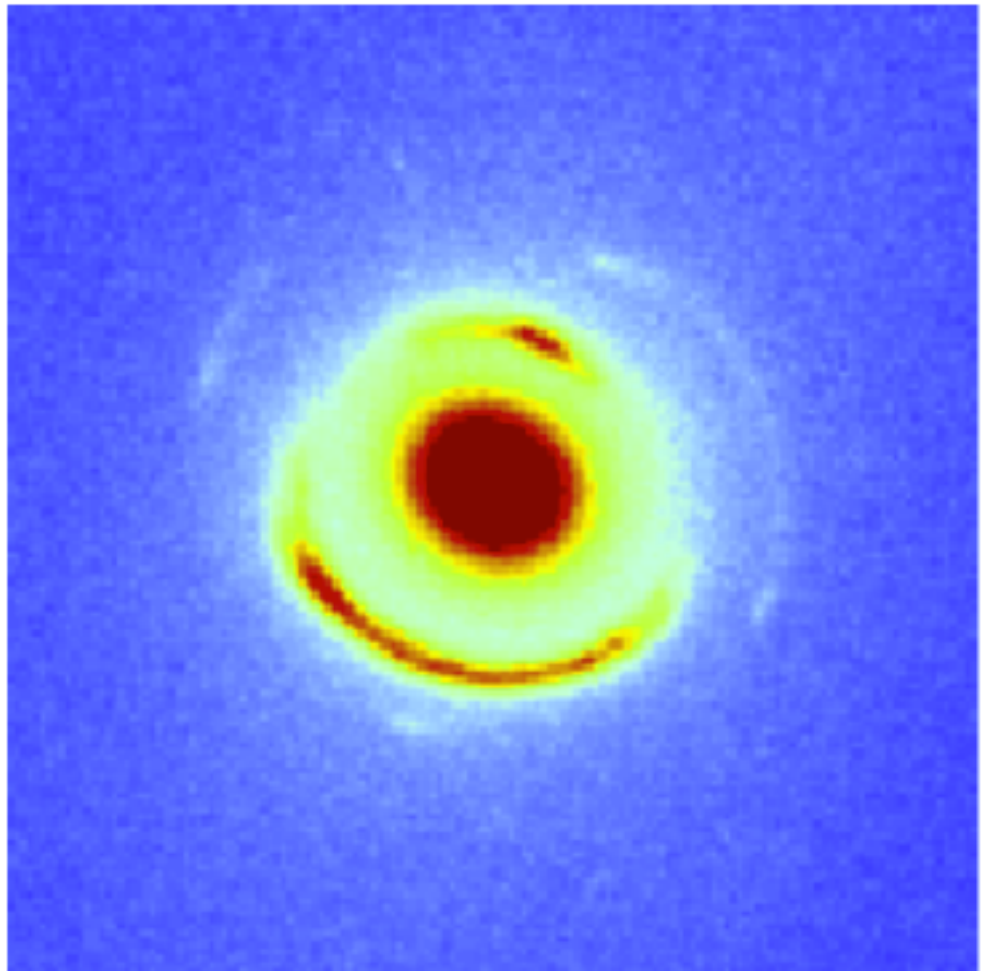


FIG. 3.— Posterior probability distribution functions of the logarithmic total density slope (γ' ; see text). The shaded region (red) indicates the joint probability for γ' , assuming isotropic stellar orbits and a Hernquist (1990) luminosity density profile. The thin solid curves refer to the 15 individual lens systems. The dashed (red) curve assumes a Jaffe (1983) luminosity density profile, leading to a several percent increase in the maximum-likelihood value of γ' . The two solid (blue) curves, indicated by $\beta = \pm 0.25$, show the probability functions for radially and tangentially anisotropic stellar orbits respectively (assuming a Hernquist profile for the stellar component). The horizontal bar indicates the 1σ intrinsic spread in γ' , corrected for the spread due to measurement errors on the stellar velocity dispersions.

THE JACKPOT LENS SDSS J0946



Gavazzi *et al.* 2008
Vegetti, *et al.* 2010
Sonnenfeld, *et al.* 2012
Collett & Auger 2014

$$z_{\text{lens}1} = 0.222$$

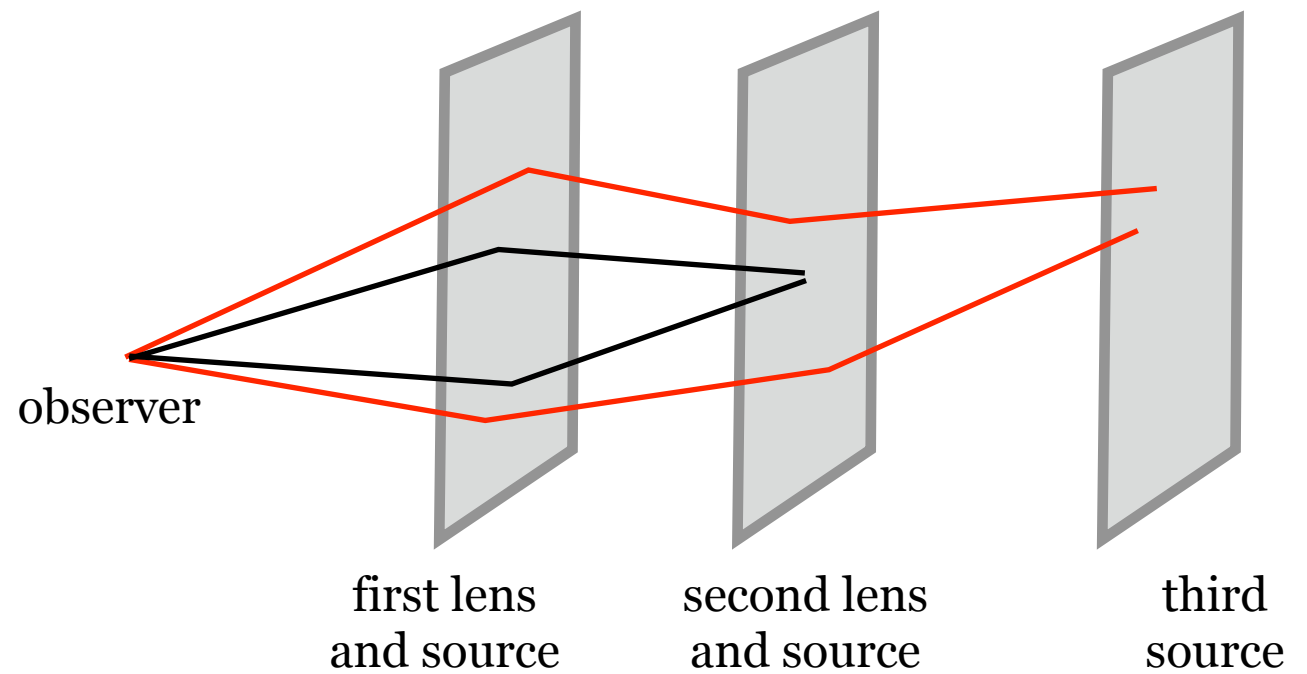
$$z_{\text{lens}2} = z_{\text{source}1} = 0.609$$

$$z_{\text{source}2} = 2.41^{+0.04}_{-0.21}$$

Double Einstein Ring

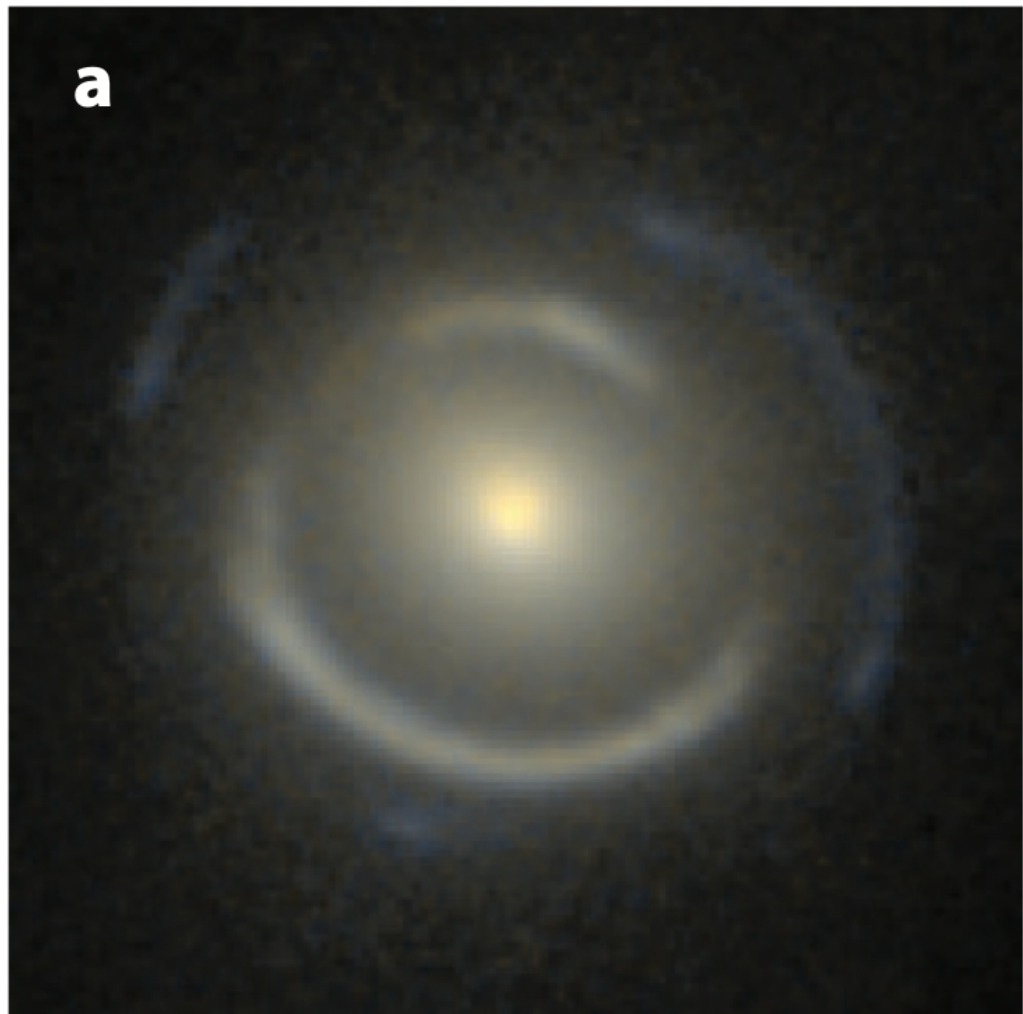
Two sources behind a large elliptical galaxy.

There is additional mass associated with the lowest redshift lensed source.



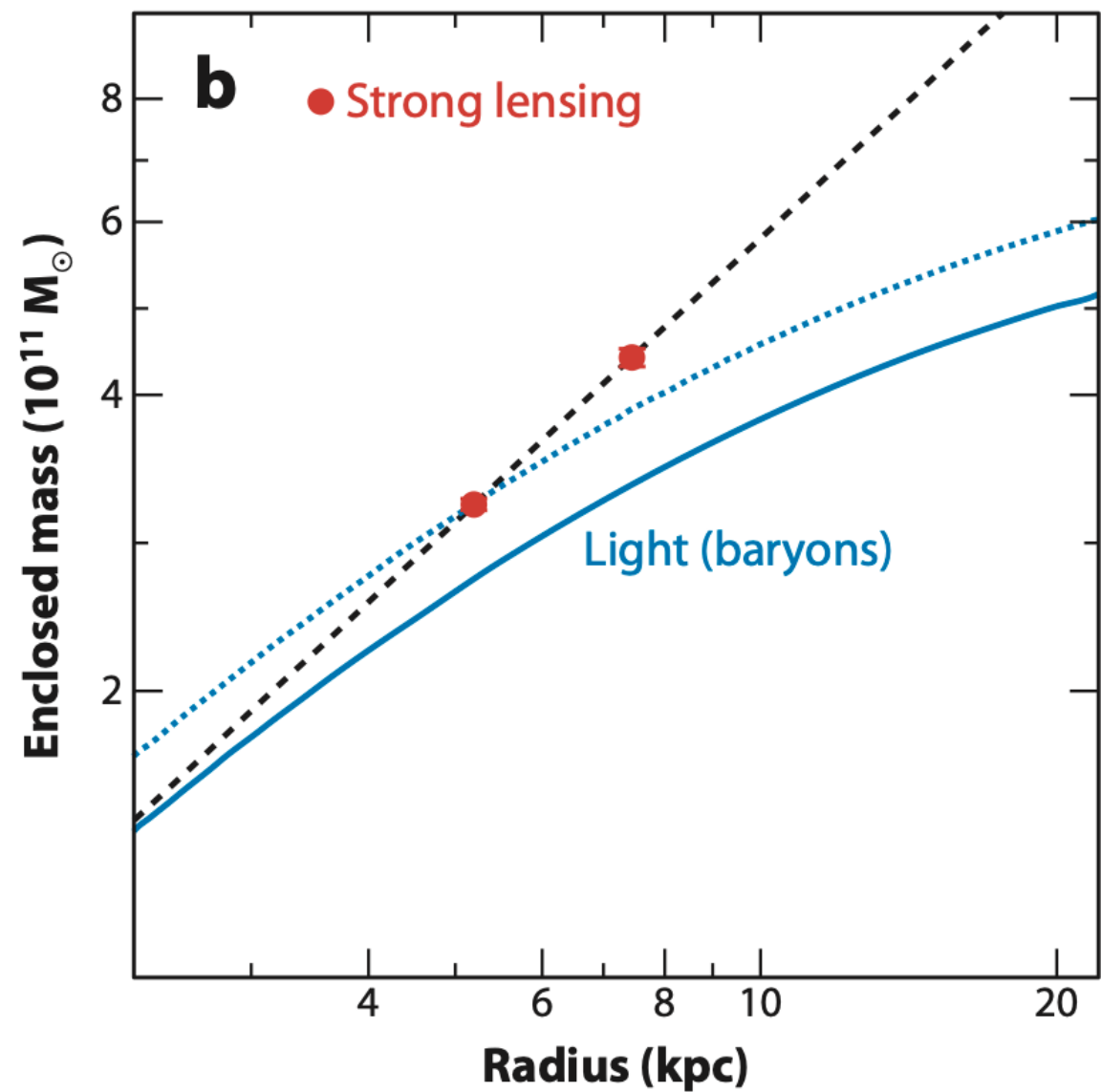
THE JACKPOT LENS SDSS J0946

SDSSJ0946 + 1006



a

Double Einstein ring J0946 + 1006



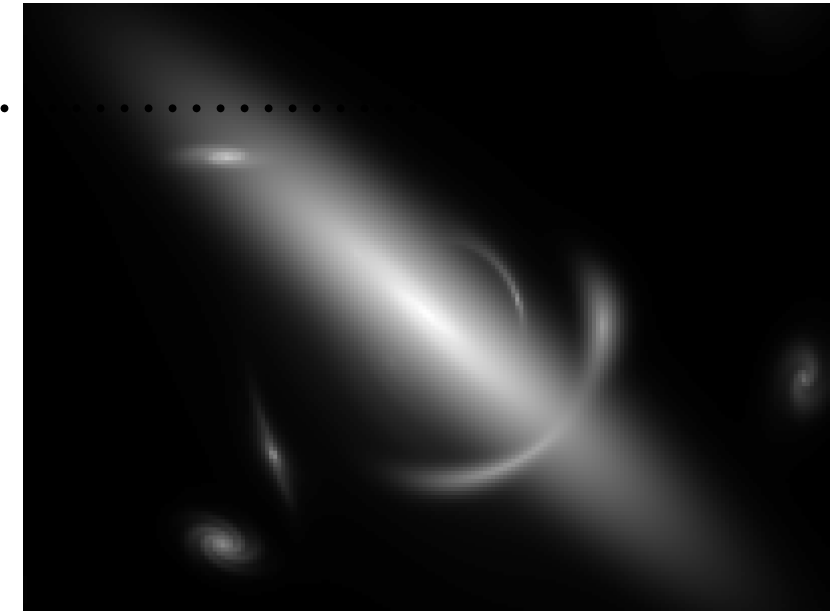
$$z_{\text{lens}1} = 0.222$$

$$z_{\text{lens}2} = z_{\text{source}1} = 0.609$$

$$z_{\text{source}2} = 2.41^{+0.04}_{-0.21}$$

JACKPOT LENSES

Double Einstein Rings



$$1 = \bar{\kappa}(R_E) = \frac{\bar{\Sigma}(R_E)}{\Sigma_{\text{crit}}(z_l, z_s)} = \frac{M(R_E)}{\mathcal{A}_\theta D_l^2 \Sigma_{\text{crit}}(z_l, z_s)} = \frac{M(R_E)}{\mathcal{A}_\theta} \left[4\pi G \frac{D_{ls}}{D_l D_s} \right]$$

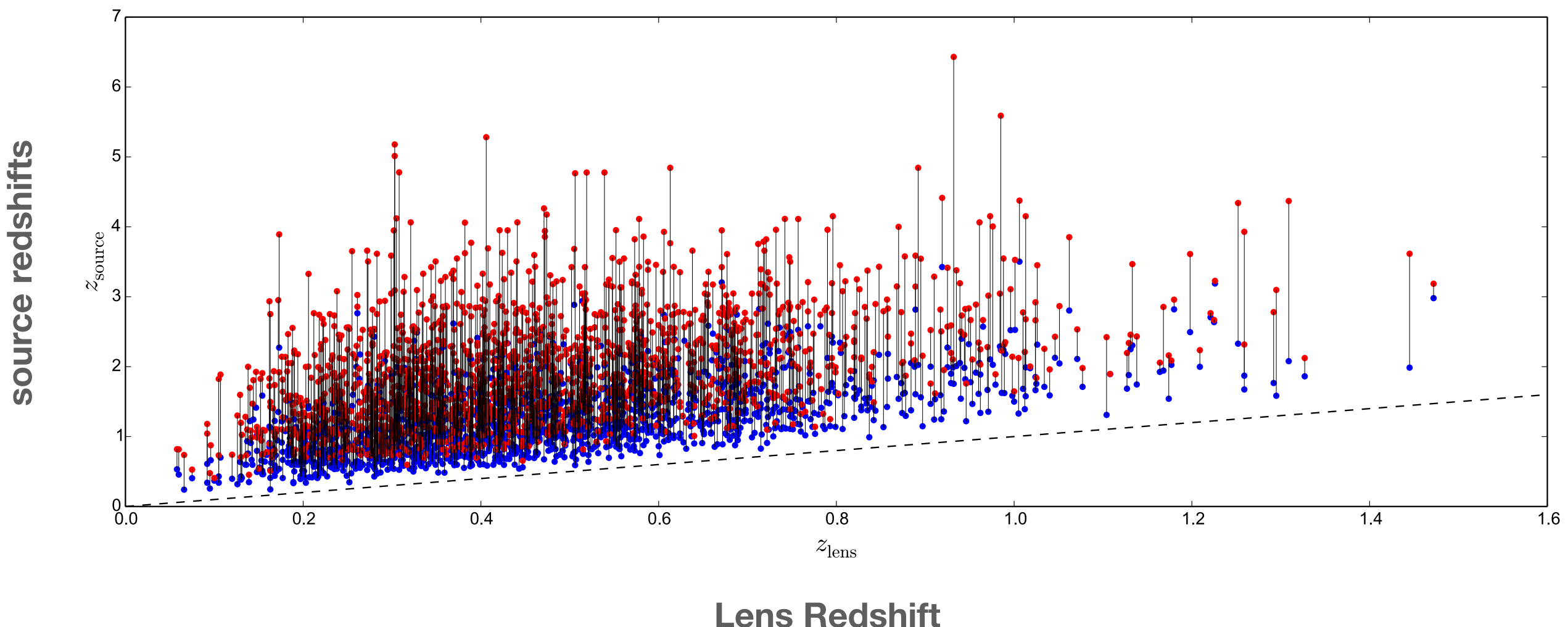
$$\frac{\mathcal{A}_1}{\mathcal{A}_2} = \left(\frac{M_1}{M_2} \right) \left[\frac{D_2 D_{l1}}{D_1 D_{l2}} \right] = \left(\frac{M_1}{M_2} \right) \beta_{12}$$

β_{12} is dependent only on cosmology and is independent of the Hubble parameter.

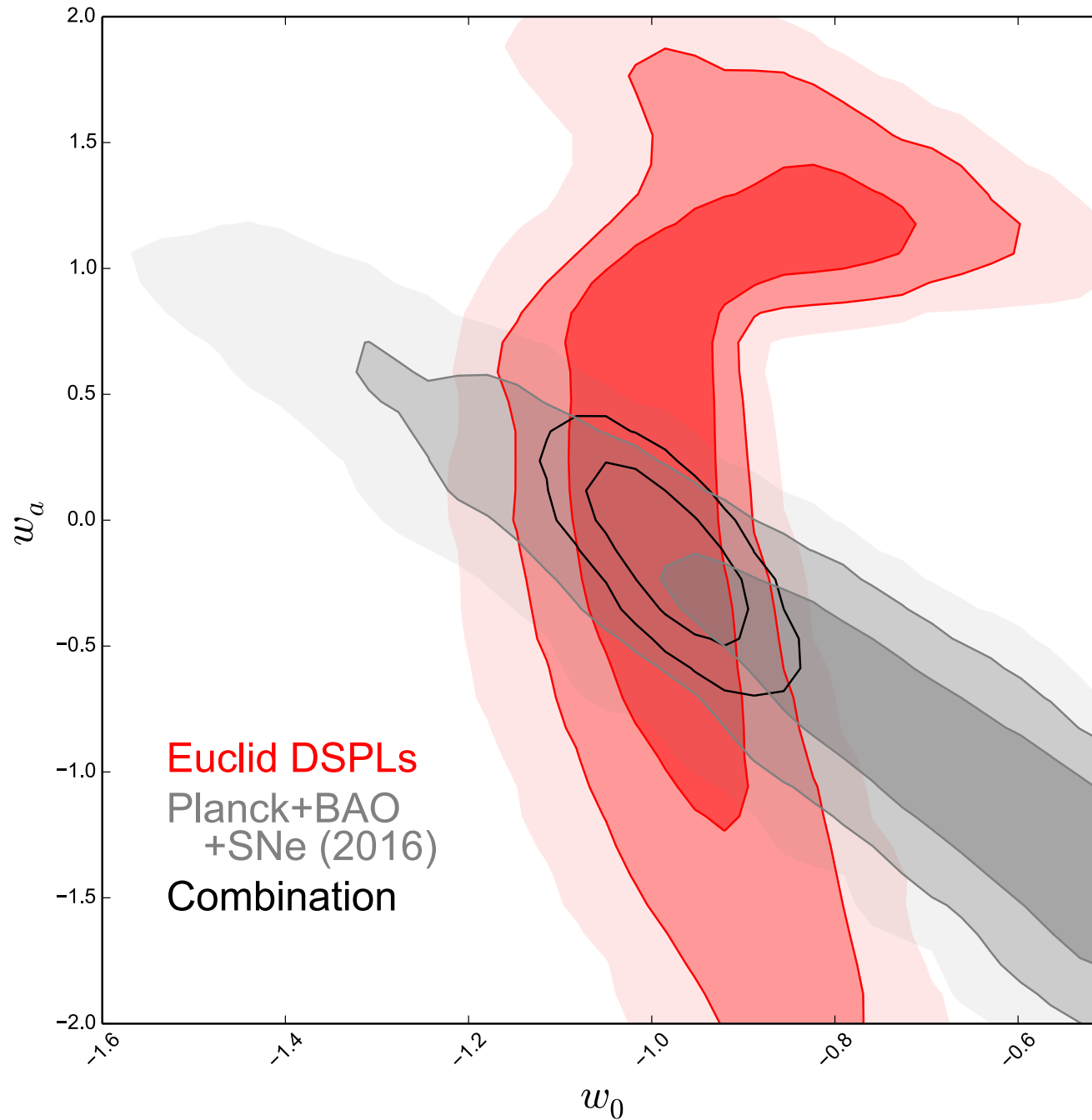
JACKPOT LENSES

Number of double Einstein rings expected in Euclid

~ 2000 double ring lenses are expected



Double Einstein Rings



Constrains on dark energy equation of state from 1,700 double rings

Constrains are very complimentary to other probes such as baryon acoustic oscillations (BAO) and type Ia supernovae.

GRAVITATIONAL LENSING

NUMERICAL SIMULATIONS

R. Benton Metcalf
2022-2023

SIMULATING LENSING ON A LARGE SCALE

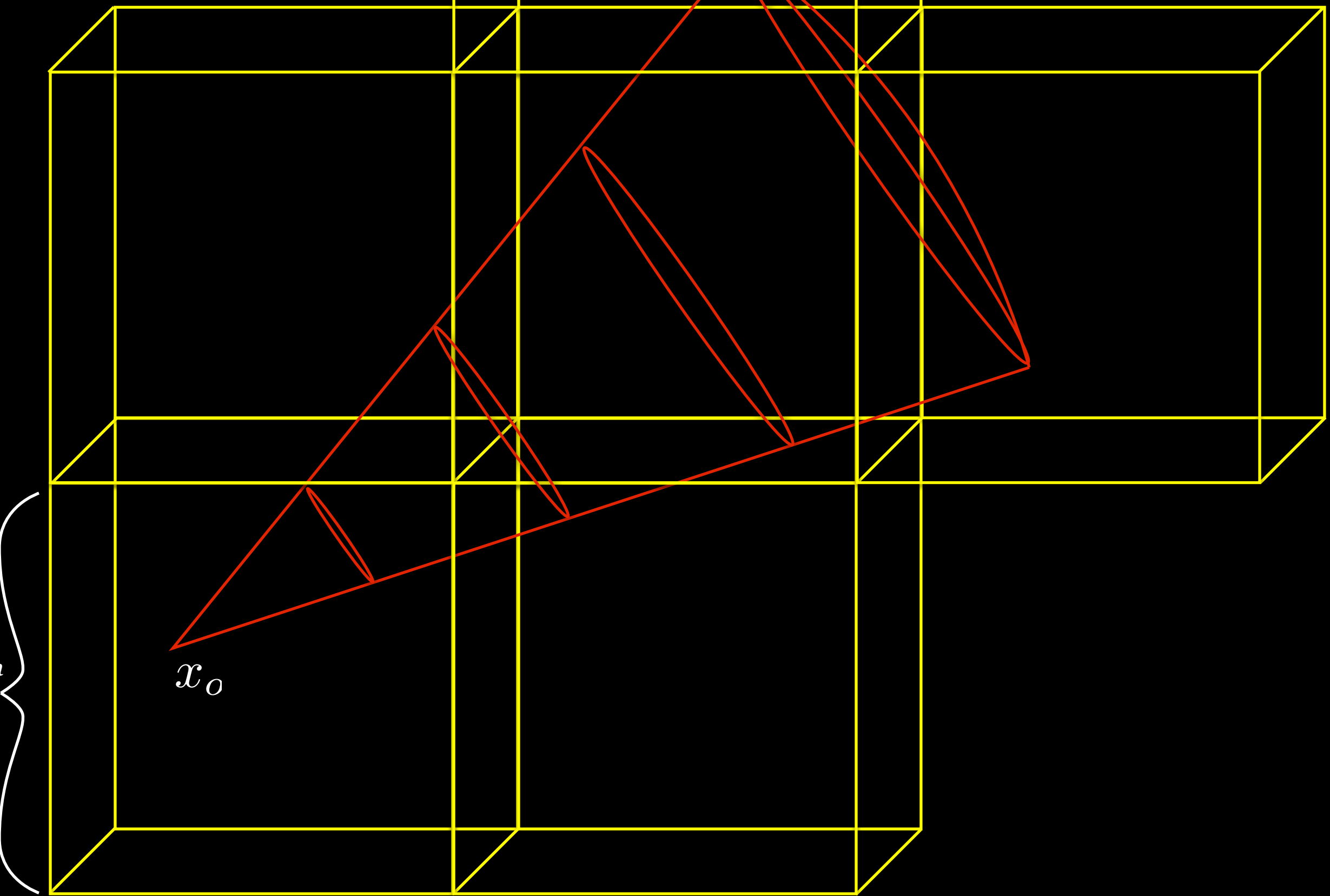
In order to predict the effects of lensing for large surveys and CMB experiments and connect them to fundamental physics one needs to use numerical simulations.

To get adequate statistical predictions one would ideally like to simulate the whole sky many times.

Simulating the sky can be relatively easily with the Born approximation and Limber's equation. However these are approximations.

More complete simulations begin with a large Nbody or hydrodynamical simulation of the Universe and propagate rays through it calculating deflections and distortions to the light bundle as they go.

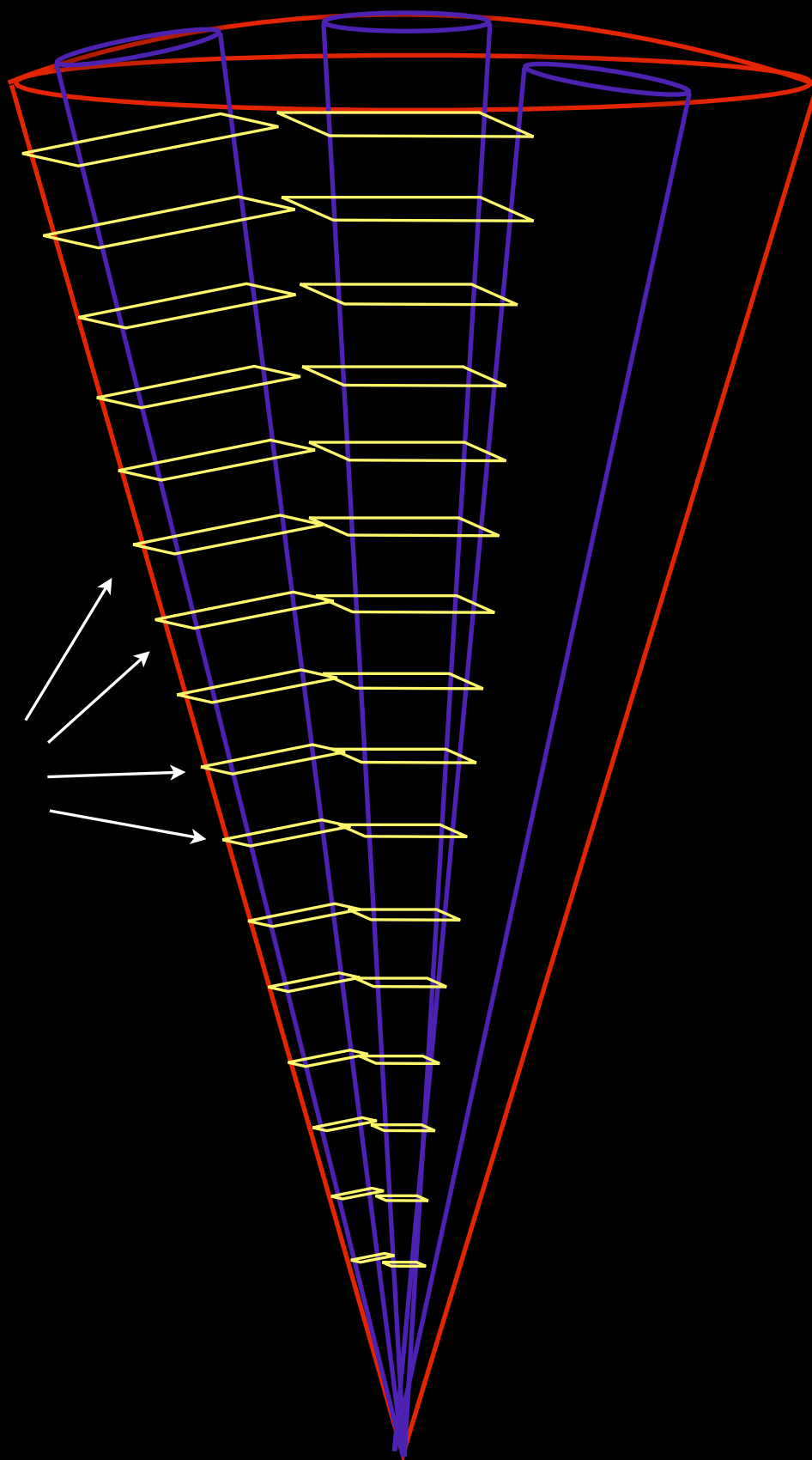
constructing light-cones



SIMULATING LENSING ON A LARGE SCALE

*ray-shooting
through the light-
cone*

lens planes

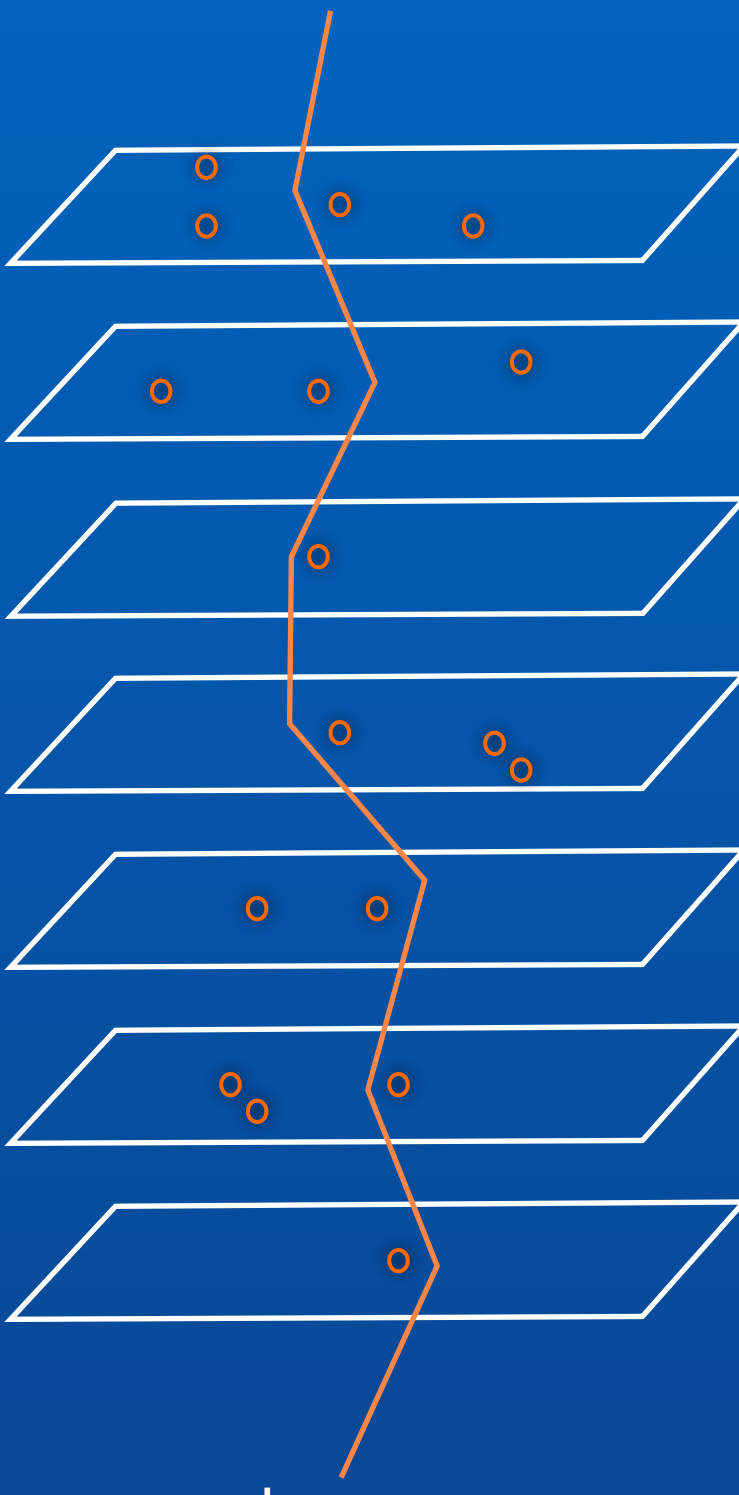


SIMULATING LENSING ON A LARGE SCALE

multi-plane lensing

source

observer



SIMULATING LENSING ON A LARGE SCALE

The deflection and distortion caused by each plane can be calculated in three ways.

By Discrete Fourier Transform (DFT or FFT)

the simulation particles are put into cells on a 2d grid

The FFT is taken and the potential is found

the deflection and shear are found in Fourier space and transformed back to real space

run time $t \sim n \log(n)$

drawbacks :

a trade-off between shot noise (particle discreteness noise) and resolution

need to do the whole thing at once which can be memory intensive

no adaptive smoothing

SIMULATING LENSING ON A LARGE SCALE

The deflection and distortion caused by each plane can be calculated in three ways.

Tree code deflection solver

particles are sorted into a tree data structure

The particles are given sizes according to the density of particles - adaptive smoothing

tree is "walked" to find the deflection and shear at each ray which don't need to be on any grid

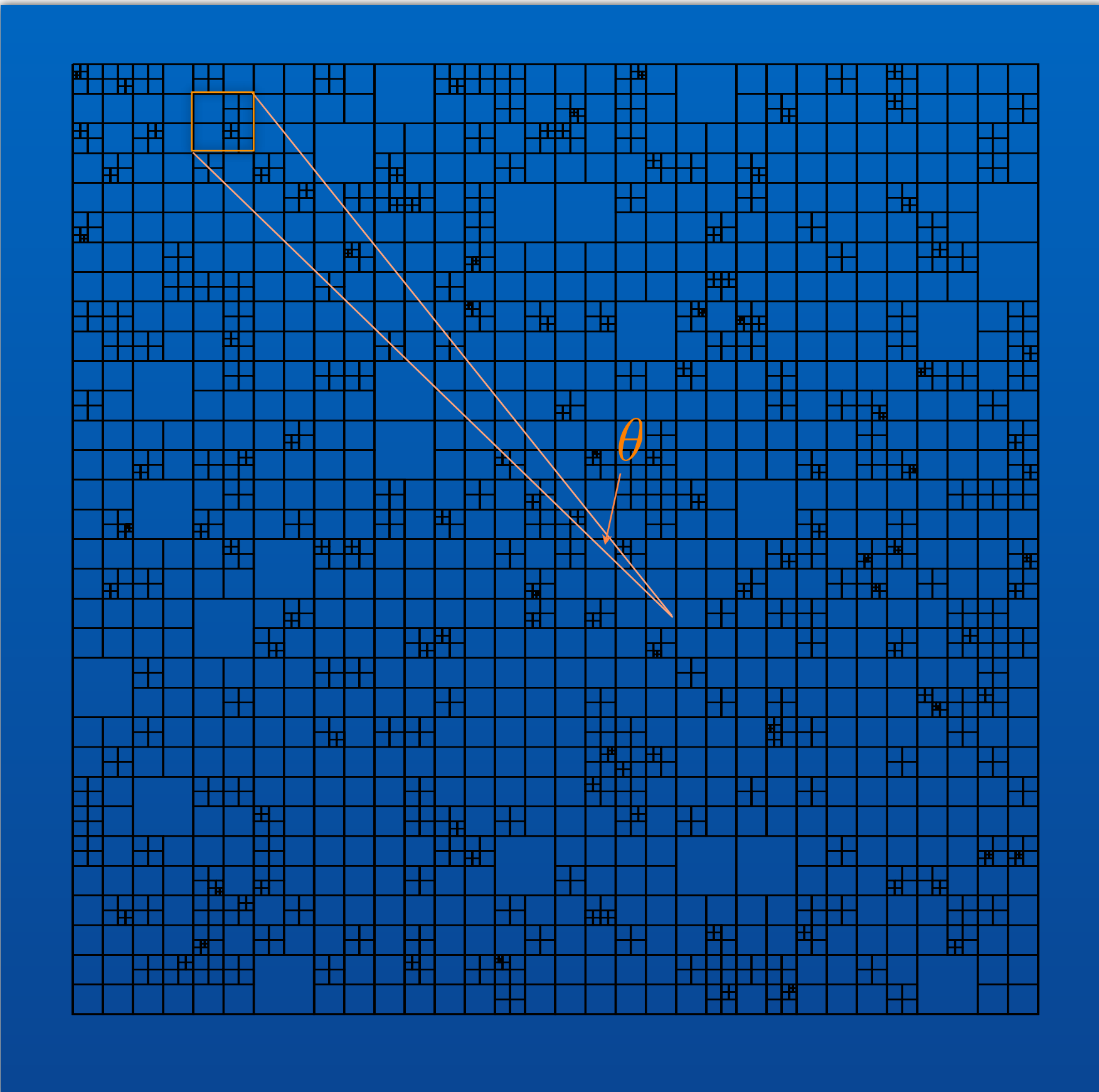
run time $t \sim n \log(n)$

drawbacks :

some initial computation needs to be done to find and store the particles sizes.

needs direct access to the particles so memory requirements are large

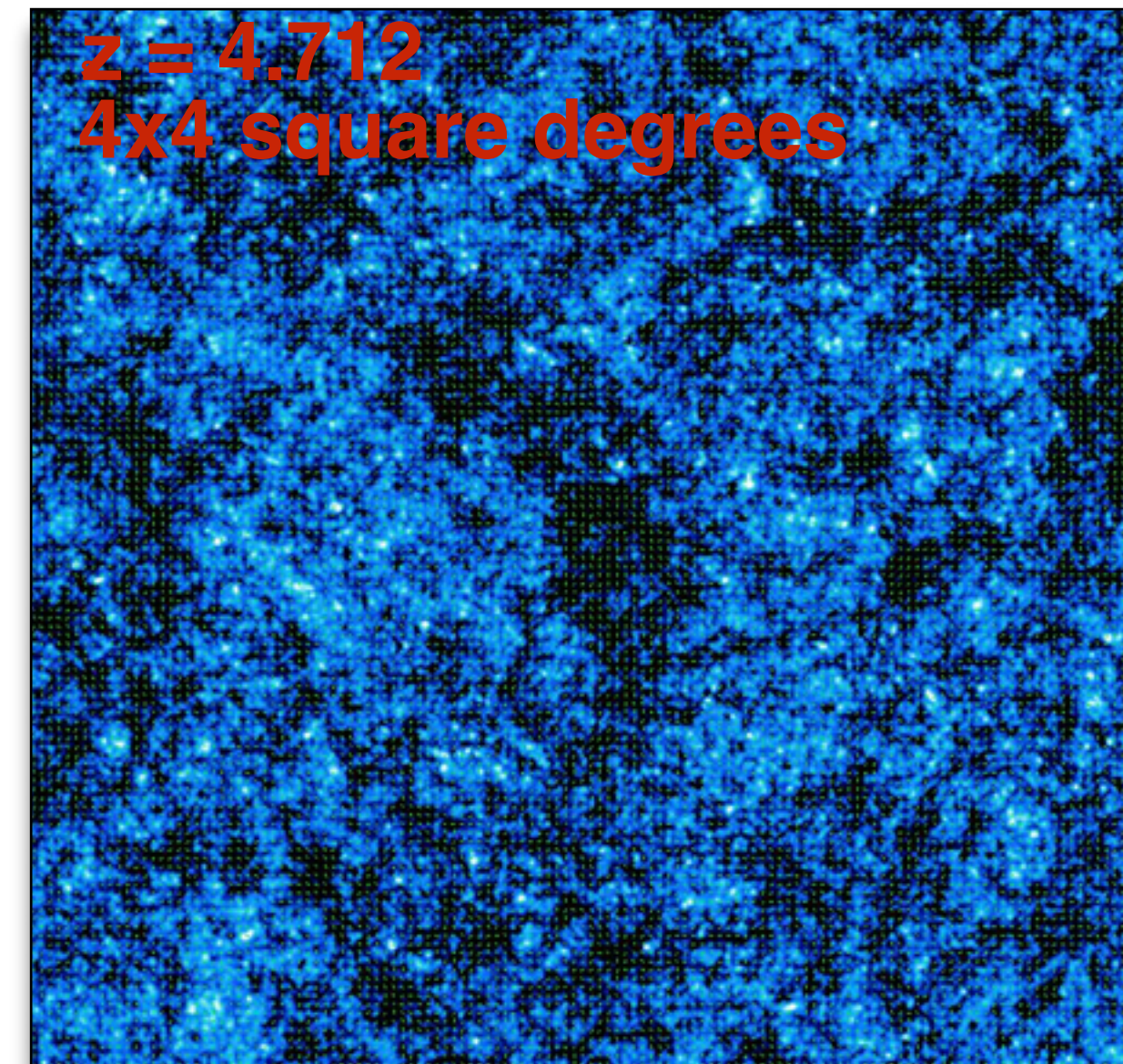
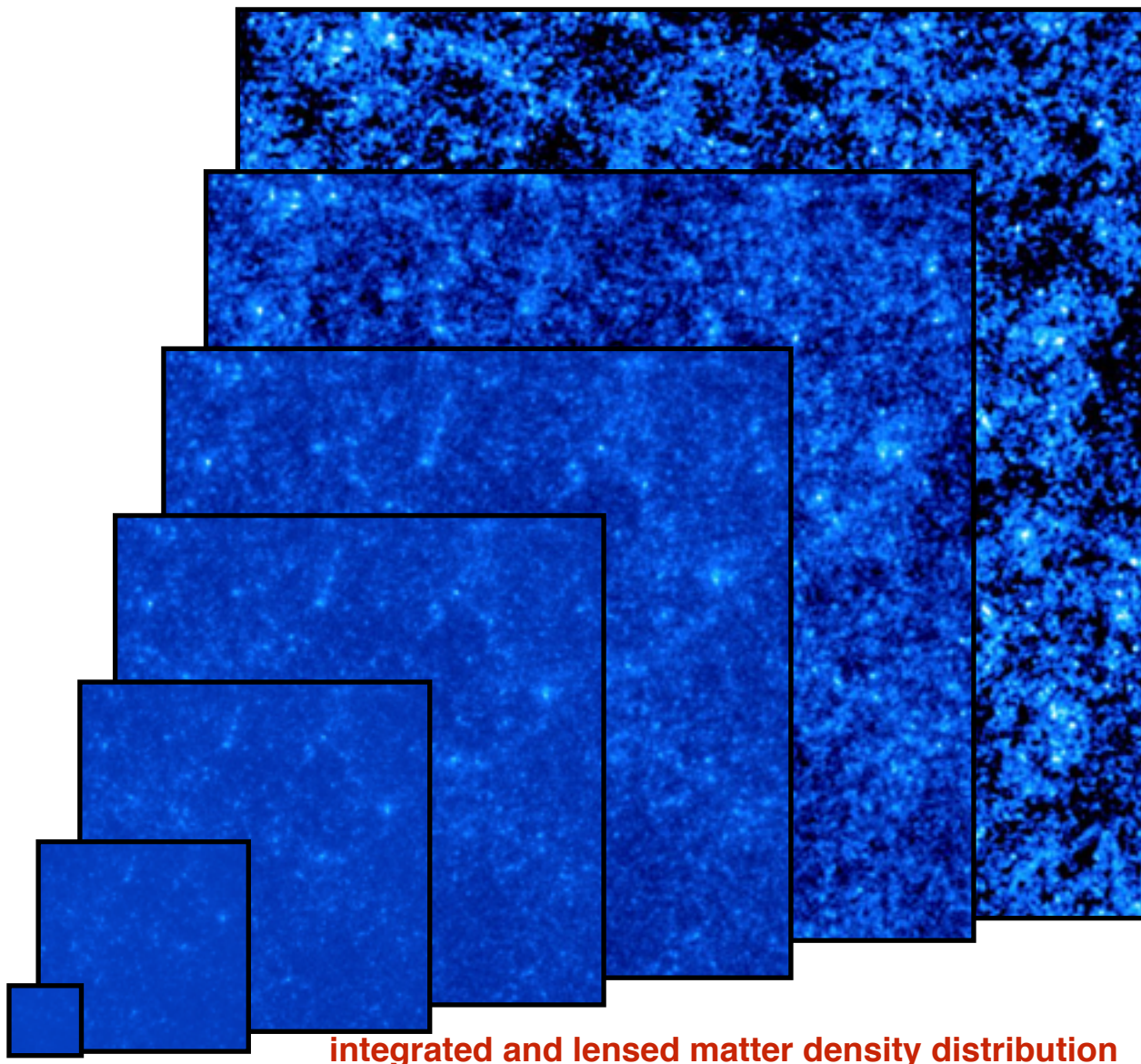
SIMULATING LENSING ON A LARGE SCALE



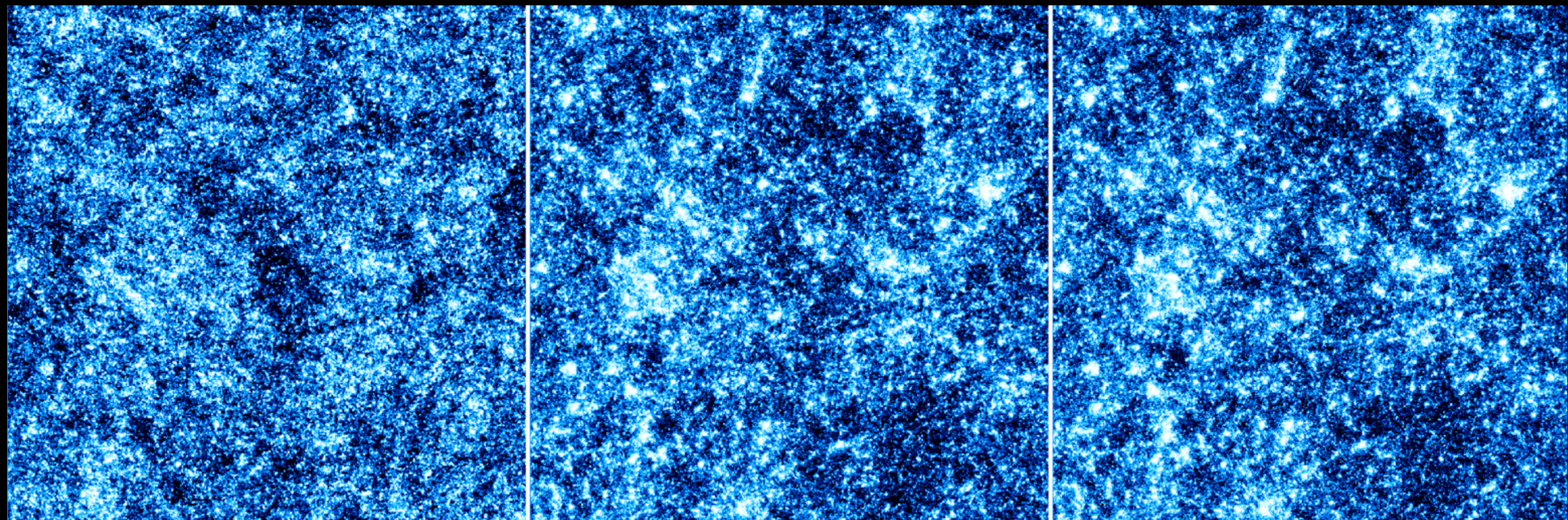
*Tree code
deflection solver*

SIMULATING LENSING ON A LARGE SCALE

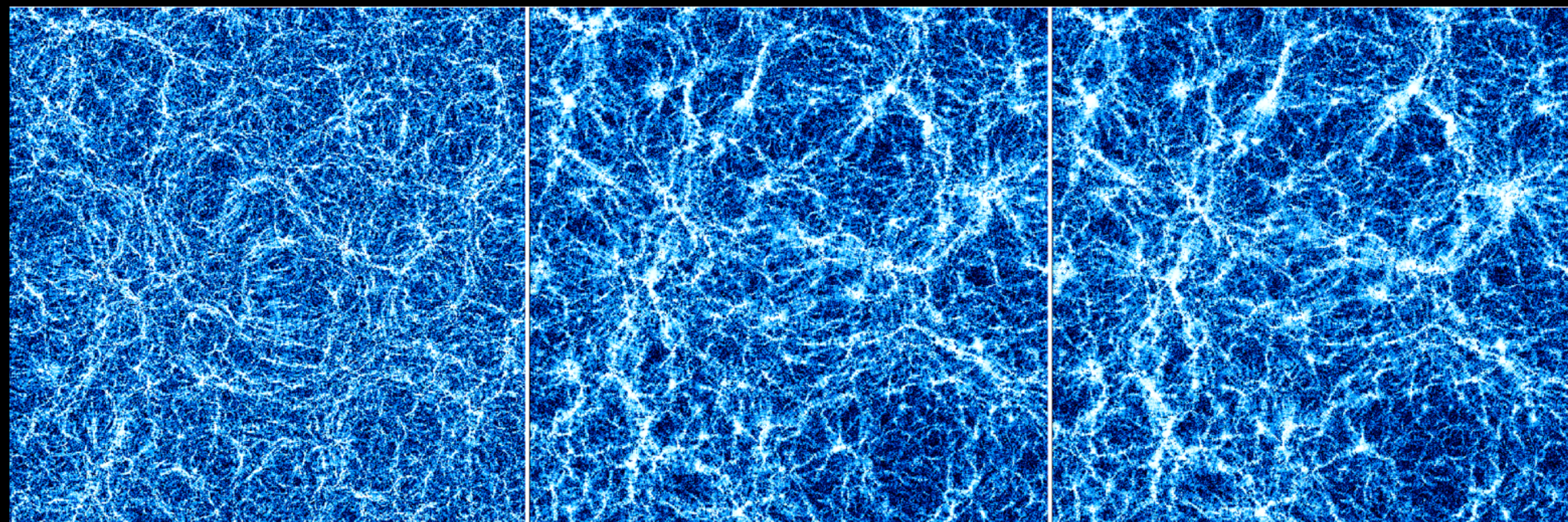
Building up the cone from the MultiDark simulation

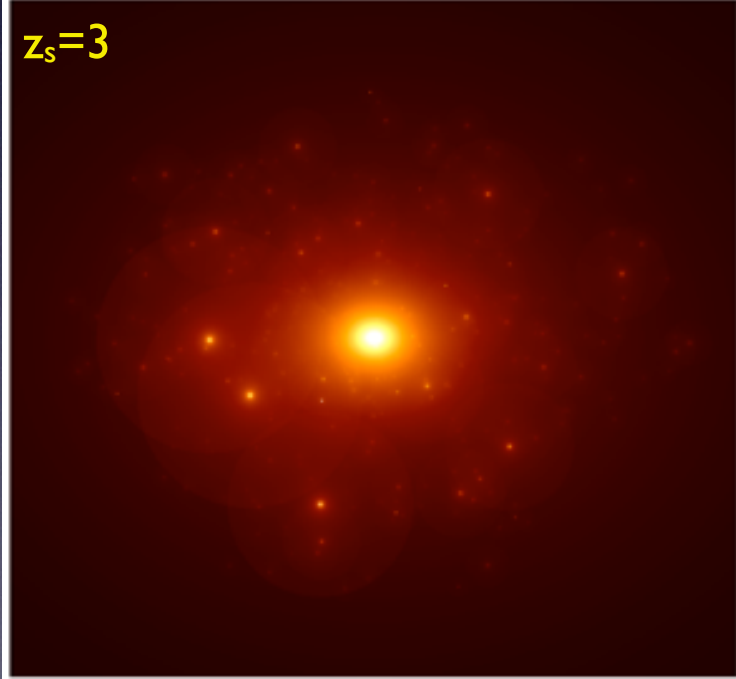
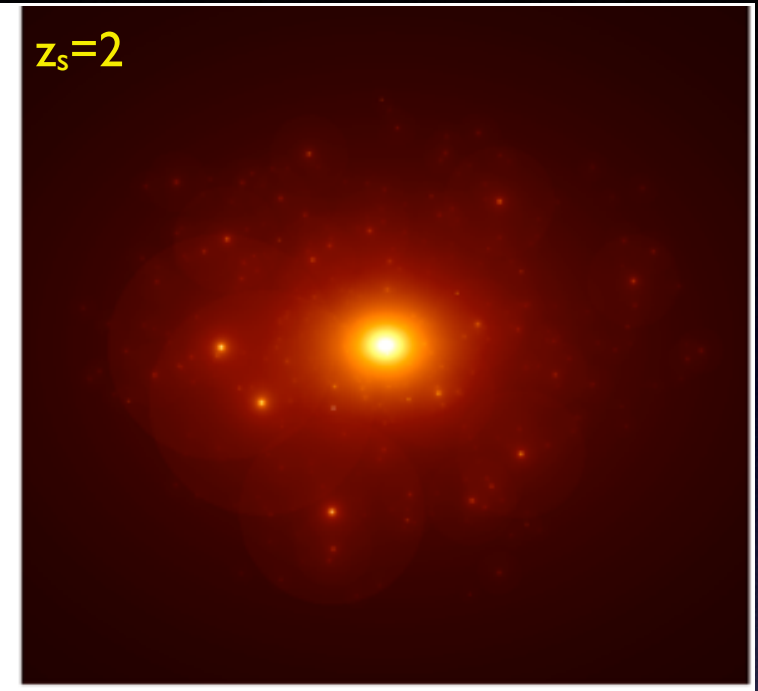
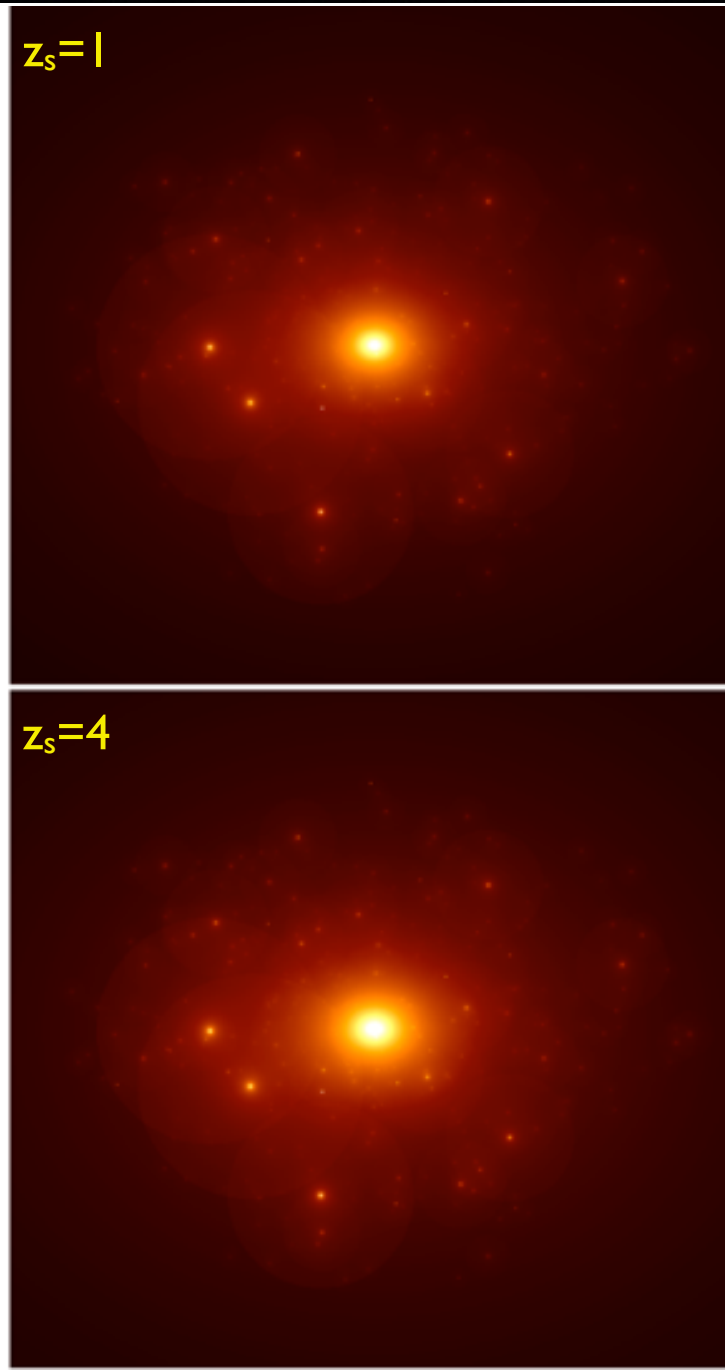
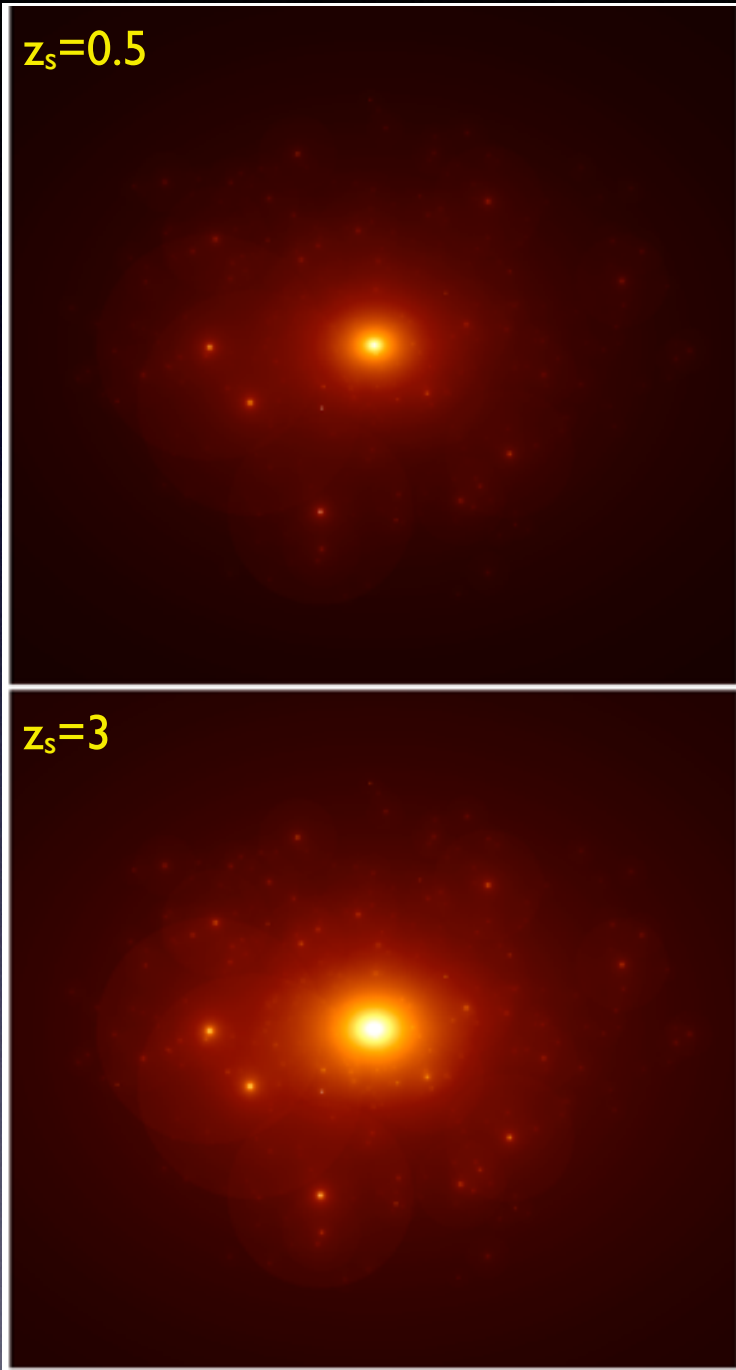


SIMULATING LENSING ON A LARGE SCALE

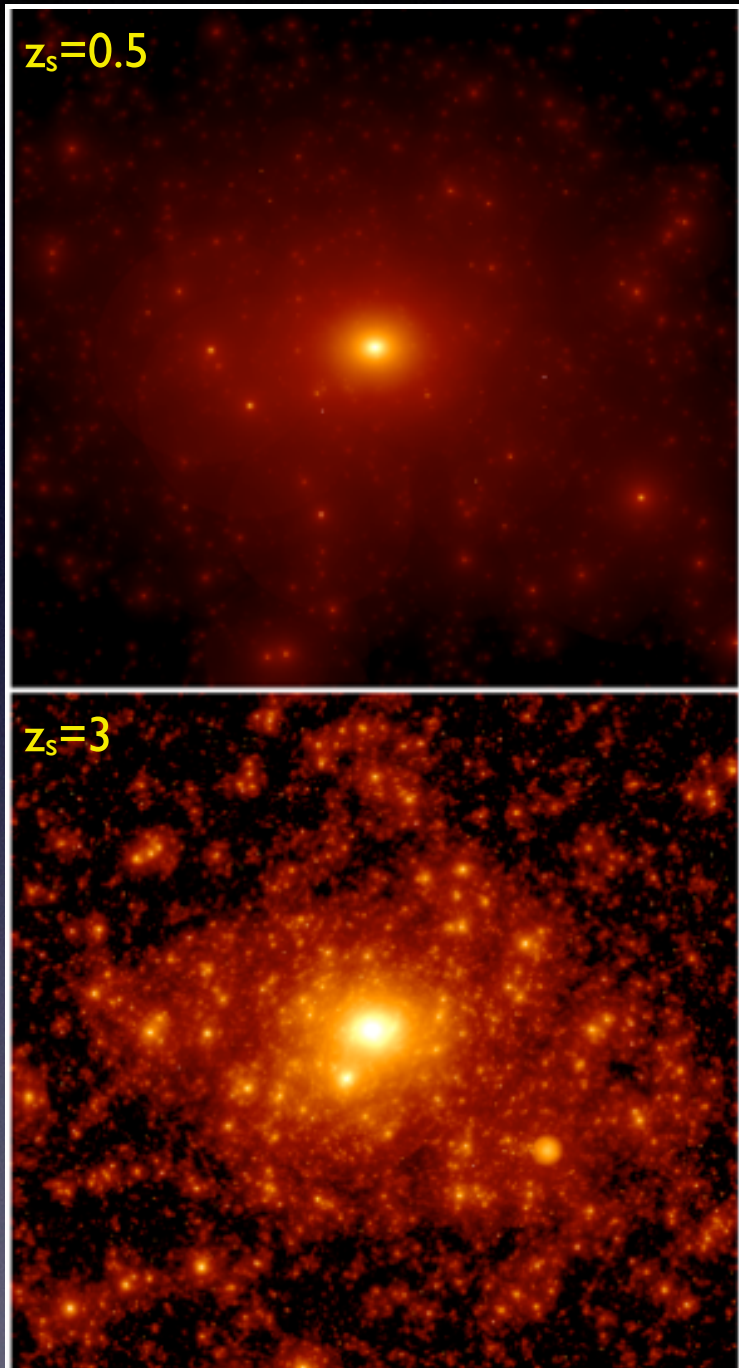


SIMULATING LENSING ON A LARGE SCALE

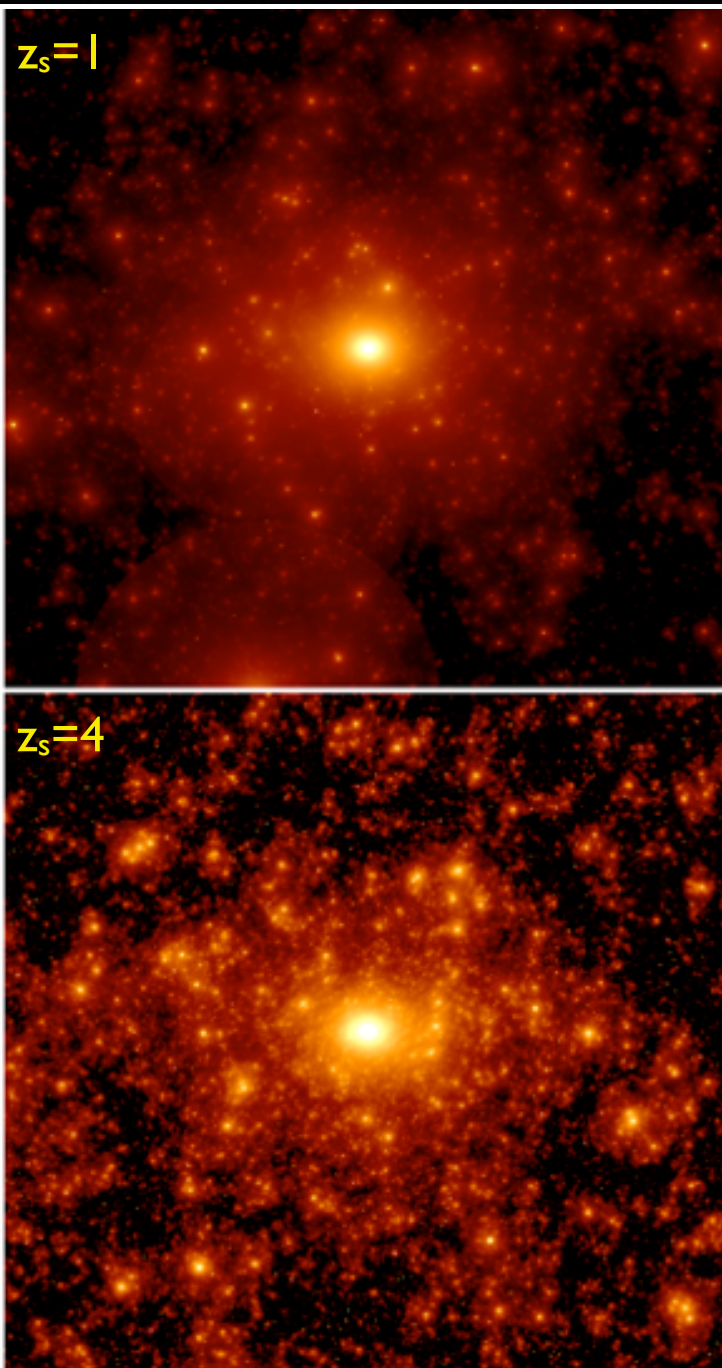




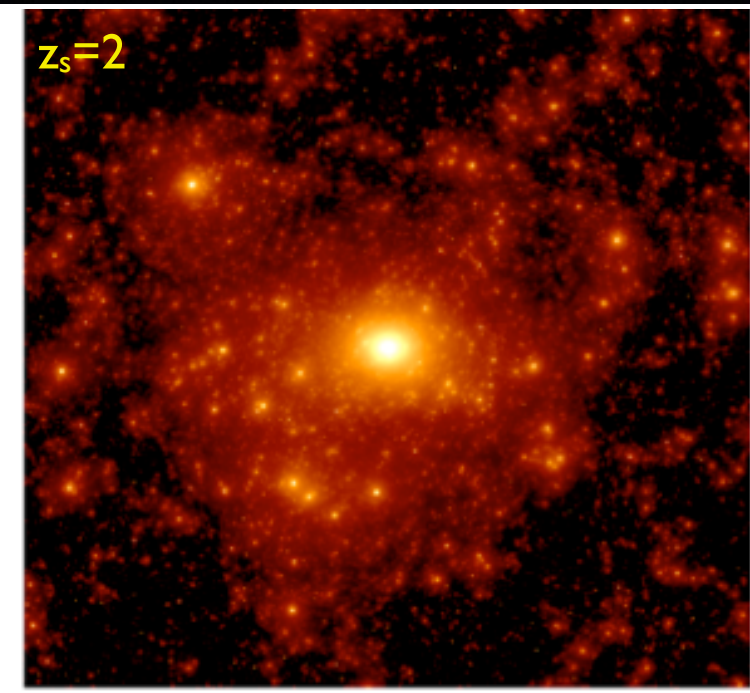
field of view = 915 arcsec
 $z_l=0.288$
 $M_{vir}=5\times 10^{14} M_{sun}/h$
cluster alone



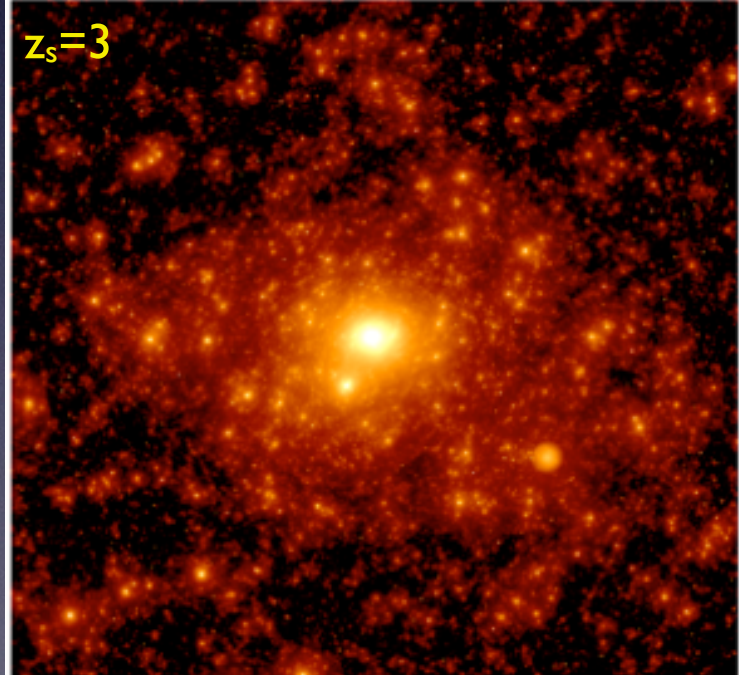
$z_s=0.5$



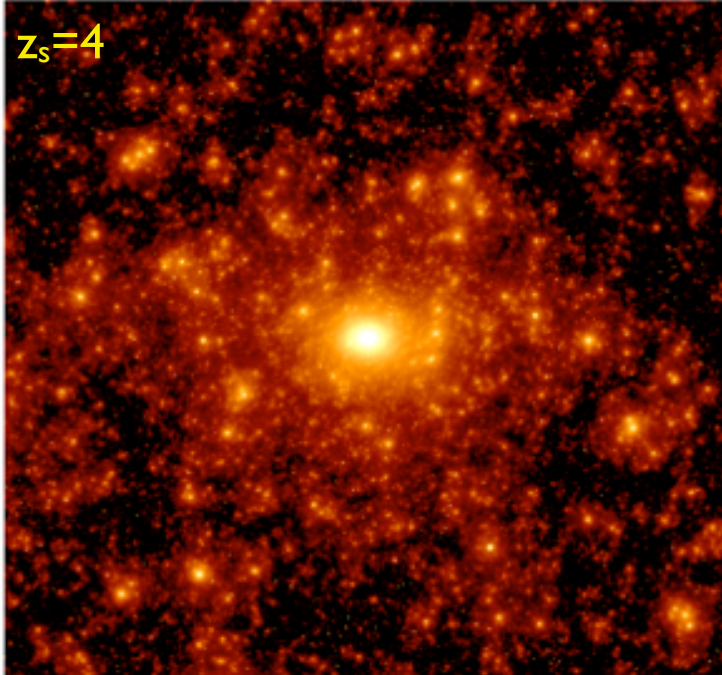
$z_s=1$



$z_s=2$



$z_s=3$



$z_s=4$

field of view = 915 arcsec

$z_l=0.288$

$M_{vir}=5\times 10^{14} M_{sun}/h$

cluster with interlopers

each simulation considers 16 planes
up to the source redshift